

## ■ Electro, Physical &amp; Theoretical Chemistry

# An Electrochemical Biosensing Platform for the SARS-CoV-2 Spike Antibody Detection Based on the Functionalised SARS-CoV-2 Spike Antigen Modified Electrode

Lokman Liv\* and Hilal Kayabay<sup>[a]</sup>

We developed an electrochemical biosensing platform using gold-clusters, cysteamine, the spike protein of the severe acute respiratory syndrome-coronavirus-2 (SARS-CoV-2) antigen and bovine serum albumin on a glassy carbon electrode able to determine the SARS-CoV-2 spike antibody. The developed biosensor could detect 9.3 ag/mL of the SARS-CoV-2 spike antibody in synthetic media in 20 min in a linear range from 0.1 fg/mL to 10.0 pg/mL. The developed method demonstrated

good selectivity in the presence of spike antigens from other viruses. Clinical samples consisting of gargle and mouthwash liquids were analyzed with both RT-PCR and the developed biosensor system to reveal the sensitivity and specificity of the proposed method. Moreover, the developed method was compared with the lateral flow immunoassay method in terms of sensitivity.

## Introduction

Since rising from Wuhan, Hubei Province of China and rapidly spreading to more than 100 countries, the unprecedented coronavirus 2019 (COVID-19) has massively disrupted public health and economies the world over.<sup>[1–3]</sup> As of 11 October 2021, almost 220 million cases and 4.6 million deaths were reported globally.<sup>[4]</sup> The disease's well-known symptoms include fever and difficulty with breathing, followed by a severe cough and other acute conditions.<sup>[5,6]</sup> However, asymptomatic cases have also contributed to COVID-19's spread and the underestimation of cases, these have made controlling the epidemic immensely difficult.<sup>[7–9]</sup> As a result, the spectacular increase of COVID-19 cases has intensified demand for methods able to rapidly, selectively and accurately diagnose the disease.<sup>[10,11]</sup>


In the literature, reported methods of diagnosing COVID-19 are based on real-time polymerase chain reaction (RT-PCR),<sup>[12–19]</sup> lateral flow assay (LFA),<sup>[20]</sup> lateral flow immunoassay (LFIA),<sup>[21–27]</sup> loop-mediated isothermal amplification (LAMP),<sup>[28–31]</sup> clustered regularly interspaced short palindromic repeats (CRISPR),<sup>[32–34]</sup> enzyme-linked immunosorbent assay (ELISA),<sup>[35]</sup> UV-visible spectroscopy,<sup>[36]</sup> computed tomography (CT) imaging,<sup>[37]</sup> plasmonic sensors,<sup>[38,39]</sup> haematological parameters,<sup>[40]</sup> and electrochemical biosensing technologies.<sup>[3,41–51]</sup> Among them, RT-PCR, despite being sensitive, selective, the most frequently used and arguably most reliable method of diagnosing COVID-19, requires experienced personnel, could be performed merely in

laboratory-scale medical institutions and is labour-intensive, time-consuming and expensive.<sup>[3,13,41,43,44]</sup> RT-PCR has even worse shown a high false-negative ratio which ranges from 20% to 67% depending on time since infection,<sup>[52,53]</sup> probably due to sampling and the quality of samples. For evidence, Wang et al.<sup>[54]</sup> studied the performance of six newly developed commercial diagnostic kits for COVID-19 and found that all of them had high limits of detection (LODs) that caused false-negative results. By some contrast, the methods based on ELISA, LFA, LFIA and UV-visible spectroscopy, despite offering significant benefits in being easy to use, cost-effective and moderately fast, have low sensitivity that also cause false-negative results.<sup>[20–27,35,36]</sup> Meanwhile, LAMP-, CRISPR- and plasmonic sensor-based methods<sup>[28–34,38,39]</sup> are highly sensitive and cost-effective but involve tedious experimental processes and require experienced personnel. Beyond those methods, CT imaging and haematological investigation are not appropriate for early or definitive diagnosis or on-site analysis.<sup>[38,55]</sup>

On the contrary, electrochemical biosensing technologies, characterised by low cost, simplicity, robustness, rapidity, high sensitivity and high selectivity, can support the diagnosis of COVID-19 by directly determining the molecular virus, the antibody produced in the organism and/or their specific proteins or segments.<sup>[56–60]</sup> It is pivotal to note that the SARS-CoV-2 antibodies may be circulating in the bodies of individuals as the vaccination has become widespread. In response, it would be good practice for antibody tests to be used to evaluate vaccine efficacy during vaccine development or clinical studies and more appropriate to use those methods in people who are not infected or have not had the disease for a long time.<sup>[61,62]</sup> Antigen-based electrochemical methods based on molecular identification (i.e. viral RNA) requiring 7 h and 29 h for sensor preparation and 40 min and 3 h for measurement provide LODs of 6900 copy/mL<sup>[41]</sup> and 200 copy/mL,<sup>[46]</sup> respectively. As for electrochemical methods based on the

[a] Dr. L. Liv, H. Kayabay

Electrochemistry Laboratory, Chemistry Group,  
The Scientific and Technological Research Council of Turkey,  
National Metrology Institute, (TUBITAK UME),  
41470, Gebze, Kocaeli, Turkey  
E-mail: lokman.liv@tubitak.gov.tr

 Supporting information for this article is available on the WWW under <https://doi.org/10.1002/slct.202200256>

detection of antigen<sup>[42–45,47–50]</sup> or antibody-based<sup>[3,44,51]</sup> spike<sup>[3,42,43,45,47,48,50,51]</sup> or nucleocapsid proteins,<sup>[42,44,49]</sup> antigen-based ones have sensor preparation times between 2 h and 25 h. Seo et al.,<sup>[43]</sup> Rahmati et al.,<sup>[47]</sup> Eissa et al.<sup>[49]</sup> and Liv et al.<sup>[50]</sup> achieved good LODs of 1 fg/mL and 100 fg/mL for the spike protein in synthetic media and clinical specimens, 0.04 fg/mL for the spike protein in synthetic media, 0.8 pg/mL for the nucleocapsid protein in synthetic media and 1 ag/mL for the spike protein in synthetic media, saliva and oropharyngeal swab samples. Fabiani et al.<sup>[42]</sup> obtained LODs of 19 ng/mL for the spike antigen and 8 ng/mL for the nucleocapsid antigen in synthetic media. By comparison, Vadlamani et al.<sup>[45]</sup> and Mojsoska et al.<sup>[48]</sup> achieved LODs of 0.1 µg/mL for the spike protein in synthetic media and 20 µg/mL for the spike protein in synthetic media and  $5.5 \times 10^5$  PFU/mL in plaque assay media, respectively. Producing the biosensor and operating the measurement with antibody-based electrochemical methods have been reported to take 3.5, 5 and 2.5 h and 15, 40 and 35 min, also respectively.<sup>[3,44,51]</sup> Although, Torrente-Rodríguez et al.,<sup>[44]</sup> who studied spike and nucleocapsid antibodies along with nucleocapsid antigen protein, gave no information regarding LODs or the dynamic range. Those methods are summarized in Table S1.

In previous studies,<sup>[3,51]</sup> our biosensing platforms using gold-clusters, cysteamine, glutaraldehyde and the SARS-CoV-2 spike antigen modified glassy carbon electrode (GCE) and gold-clusters, mercaptoethanol and the SARS-CoV-2 spike antigen modified GCE could detect 0.01 ag/mL and 0.03 fg/mL of the spike antibody in synthetic media. By extension, in the study reported here, we aimed to develop a simple, rapid, accurate, cost-effective, sensitive, selective method of diagnosing COVID-19 by functionalising the SARS-CoV-2 spike antigen protein (S-AG) with N-(3-dimethylaminopropyl)-N'-ethylcarbodiimide hydrochloride (EDC) and N-hydroxysuccinimide (NHS) instead of glutaraldehyde. We modified the functionalised S-AG (f-S-AG) on cysteamine (CysNH<sub>2</sub>) and gold-clusters modified GCE and blocked gaps on the biosensor surface with bovine serum albumin (BSA)-altogether, the product was BSA/f-S-AG/CysNH<sub>2</sub>/Au/GCE- and used the biosensor to determine the SARS-CoV-2 spike antibody (S-AB) in spiked-saliva and -oropharyngeal swab and RT-PCR approved real samples.

## Results and Discussion

### Characterisation of the sensors

The preparation steps of the biosensing platform, BSA/f-S-AG/CysNH<sub>2</sub>/Au/GCE, and voltammetrically measuring scheme for S-AB are shown in Figure 1.

The characterisation of the electrodes after each modification, as evaluated with cyclic voltammetry (CV), scanning electron microscopy (SEM) and energy dispersive X-ray spectroscopy (EDX), indicated clear consistency with findings reported in the literature.<sup>[3,60]</sup> First, CV measurements were recorded for the GCE, Au/GCE, CysNH<sub>2</sub>/Au/GCE, f-S-AG/CysNH<sub>2</sub>/Au/GCE and BSA/f-S-AG/CysNH<sub>2</sub>/Au/GCE electrodes in 1 mM of K<sub>3</sub>[Fe(CN)<sub>6</sub>], 1 mM of K<sub>4</sub>[Fe(CN)<sub>6</sub>] and 0.1 M of KCl with a scan rate of 50 mV/

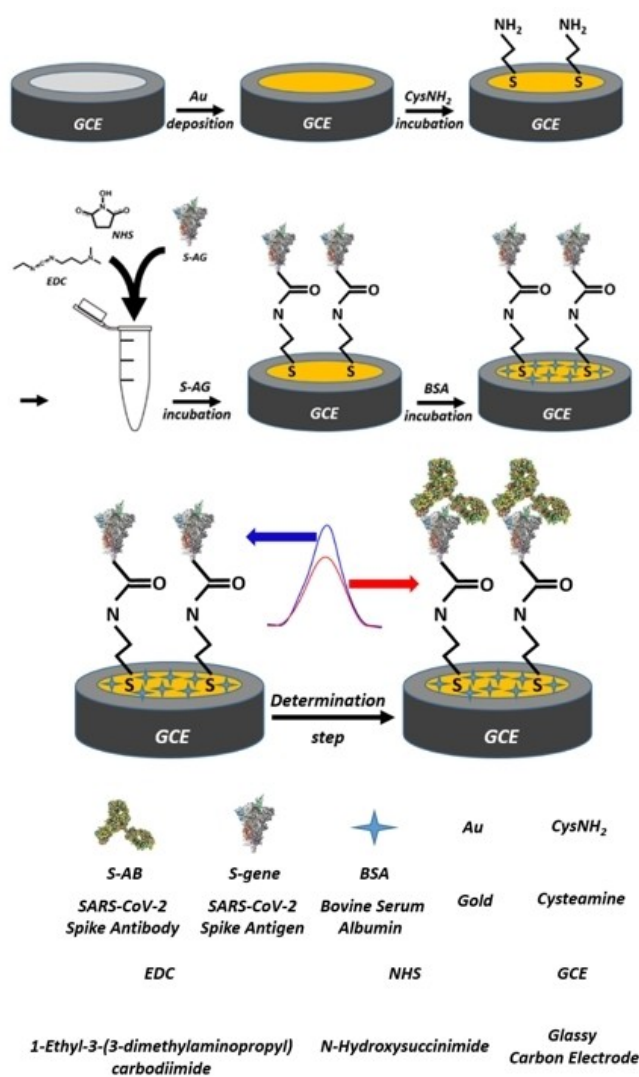
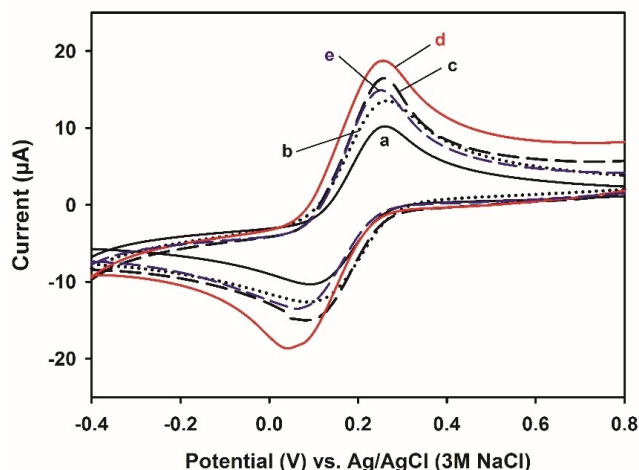


Figure 1. The preparation steps of the biosensing platform, BSA/f-S-AG/CysNH<sub>2</sub>/Au/GCE, and voltammetrically measuring scheme for S-AB.

s (Figure 2). The characterisations of gold-clusters and CysNH<sub>2</sub> deposited on the GCE were the same as in our previous study.<sup>[3]</sup> Briefly, the peak heights of the redox couple substantially increased owing to the enlarged surface area and enhanced electron transfer rate of Au/GCE (Figure 2b), and the peak heights continued to increase after the incubation of CysNH<sub>2</sub> on Au/GCE (Figure 2c), which we attributed to the electrostatic attraction and interaction between the redox couple and the amine sites of CysNH<sub>2</sub>/Au/GCE.<sup>[3,60]</sup> After the f-S-AG was modified on the surface of CysNH<sub>2</sub>/Au/GCE, the peak heights of the redox couple reached their greatest value (Figure 2d), partly due to the positively charged Au surface that attracted the negatively charged redox couple. Ultimately, the peak heights decreased once the positively charged Au surface was blocked by BSA, which hindered the redox couple from reaching the surface of BSA/f-S-AG/CysNH<sub>2</sub>/Au/GCE (Figure 2e).

To identify the elemental composition of the surfaces of the electrodes, SEM images and EDX spectra for the bare GCE, Au/



**Figure 2.** Cyclic voltammograms of (a) GCE, (b) Au/GCE, (c) CysNH<sub>2</sub>/Au/GCE, (d) *f*-S-AG/CysNH<sub>2</sub>/Au/GCE and (e) BSA/*f*-S-AG/CysNH<sub>2</sub>/Au/GCE in 1 mM of K<sub>3</sub>[Fe(CN)<sub>6</sub>], 1 mM of K<sub>4</sub>[Fe(CN)<sub>6</sub>] and 0.1 M of KCl with a scan rate of 50 mV/s.

GCE, CysNH<sub>2</sub>/Au/GCE, *f*-S-AG/CysNH<sub>2</sub>/Au/GCE and BSA/*f*-S-AG/CysNH<sub>2</sub>/Au/GCE were taken, as shown in Figure 3 and Fig-

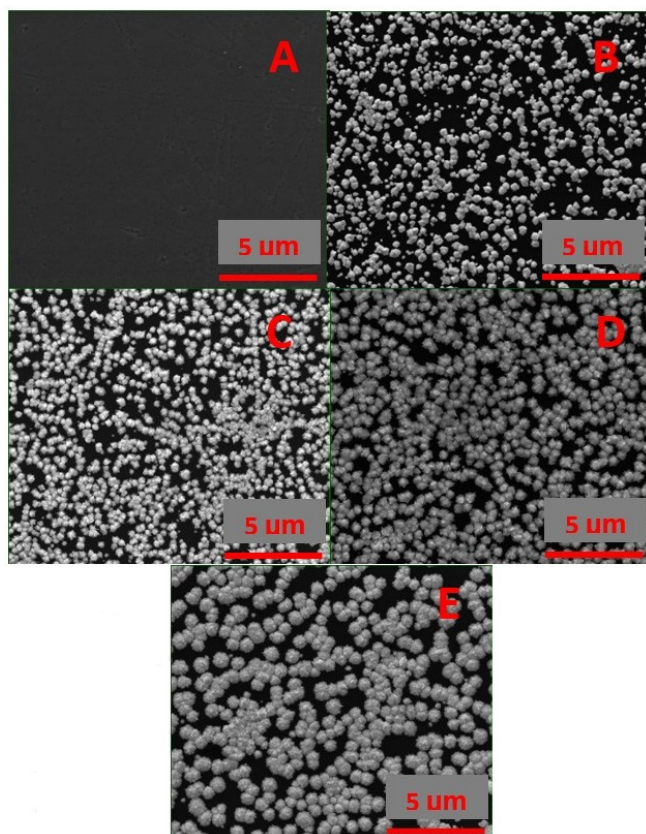


**Figure 3.** SEM images of (A) bare GCE, (B) Au/GCE, (C) CysNH<sub>2</sub>/Au/GCE, (D) *f*-S-AG/CysNH<sub>2</sub>/Au/GCE and (E) BSA/*f*-S-AG/CysNH<sub>2</sub>/Au/GCE (SEM analysis: 20 kV voltage, 4.0 spot value, ETD detector).

ure S1, respectively. A smooth SEM image (Figure 3A) and an EDX spectrum (Figure S1A) consisting of only carbon (85.2%) and oxygen (14.8%) were obtained for the bare GCE. After we deposited gold-clusters onto the GCE's surface, roundish structures formed there, and more than half (63.8%) of the surface became covered by gold-clusters, as shown in Figure 3B and Figure S1B, respectively. As illustrated in Figs. 3B–E, because the bonding took place on the surface of the gold-clusters, the particle sizes increased with each subsequent modification, and the bright, roundish structures of the gold-clusters became grey due to the decrease in conductivity especially with recent modifications. Because CysNH<sub>2</sub> was chemisorbed from sulphur terminals by gold-clusters, nitrogen peaks (4.7%) emerged in the EDX spectrum owing to the remaining nitrogen sites on the electrode surface (Figure S1C). Unlike in our previous study, a low amount of sulphur (0.2%) on the CysNH<sub>2</sub>/Au/GCE electrode can be attributed to the use of a threefold greater concentration of CysNH<sub>2</sub>. Because the S-AG immobilised to the surface at amine terminals of CysNH<sub>2</sub> by means of EDC and NHS, the amount of nitrogen on the surface of CysNH<sub>2</sub>/Au/GCE decreased from 4.7% to 2.7% on the *f*-S-AG/CysNH<sub>2</sub>/Au/GCE electrode (Figure S1D). With the immobilisation of BSA on *f*-S-AG/CysNH<sub>2</sub>/Au/GCE, the amount of nitrogen on the surface increased, thereby indicating that proteinic structures had fastened to the surface (Figure S1E). Critically, the decrease in the amount of Au on the surface after each modification of the Au/GCE surface indicates that the modifications were successful. Beyond that, largely aligned CV, SEM and EDX measurements revealed that all the steps for electrode modification had been effectively applied to produce the biosensing platform.

### CV measurements

The redox behaviour of the biosensor and the added SARS-CoV-2 spike antibody were extensively investigated in 0.01 M (pH 7.5) of PBS solution. The biosensor had two oxidation peaks at 0.30 V and 0.70 V and two reduction peaks at 0.77 V and -0.16 V. However, only the peak at 0.70 V decreased proportionally with the increasing amount of the SARS-CoV-2 spike antibody (Figure S2). To identify the electrode reaction mechanism, CV scans were recorded at increasing scan rates, and the peak height ( $I_p$ ,  $\mu\text{A}$ ) – scan rate ( $v$ , mV/s), the peak height – the square root of scan rate ( $\sqrt{v}$ ,  $\sqrt{\text{mV/s}}$ ) and the logarithm of peak height ( $\log(I_p)$ ,  $\mu\text{A}$ ) – the logarithm of scan rate ( $\log(v)$ , mV/s) were plotted and the related equations obtained were  $I_p = 0.0121v + 0.3003$  ( $R^2 = 0.9999$ ) and  $\log(I_p) = 0.9201 \log(v) - 1.6747$  ( $R^2 = 0.9996$ ), respectively. The linearity of  $I_p - v$  curve, the non-linearity of  $I_p - \sqrt{v}$  curve and the slope of  $\log(I_p) - \log(v)$  curve close to 1 suggest that the system accommodated an adsorption-controlled electrode reaction (Figure S3).

### Optimisation studies

Pivotal parameters for preparing the biosensor were examined in the presence of 100 fg/mL of S-AB. Among the results, the

concentration of CysNH<sub>2</sub>, S-AG, the ratio of EDC to NHS (200 mM each) and the binding time of CysNH<sub>2</sub>, S-AG, BSA and S-AB were optimised as to be 60 mM, 1 µg/mL, 6 µL/4 µL, 30 min, 15 min, 20 min and 15 min, as appear in Figure S4 for detecting S-AB in synthetic and spiked-real samples. All of the measurements were carried out in 0.01 M (pH 7.5) of PBS solution, because the pH of bodily fluids is generally neutral.

The MERS-CoV spike antigen (M-S-AG), influenza A spike antigen (InFA) and *Streptococcus pneumoniae* antigen (Pneu) were separately attached on CysNH<sub>2</sub>/Au/GCE and blocked with BSA – they were labelled BSA/f-M-S-AG/CysNH<sub>2</sub>/Au/GCE, BSA/f-InFA/CysNH<sub>2</sub>/Au/GCE and BSA/f-Pneu/CysNH<sub>2</sub>/Au/GCE – to evaluate the selectivity of the proposed method. As a result, the fabricated sensors showed no significant response to 100 fg/mL of S-AB (Figure S5). Interference effects using 5% variation in peak height as a criterion were evaluated using anions, enzymes and compounds that exist in saliva with 100 fg/mL of S-AB, as shown in Table 1. The results show that the good selectivity of the developed method.

### Method validation

Since the developed biosensor consists of heteroatoms arise from the surface of the S-AG, the obtained current is capacitive decreasing with the addition of S-AG due to the interaction between S-AB and S-AG. The SWV voltammograms and calibration curve for the detection of S-AB are shown in Figure 4.

$\Delta I_p$  values were obtained by subtracting the peak height of S-AB from the peak height of BSA/f-S-AG/CysNH<sub>2</sub>/Au/GCE. The LOD and analytical range of the developed method for S-AB were respectively 9.3 ag/mL (i.e. from the blank signal) and 0.1 fg/mL–10 pg/mL in 0.01 M (pH 7.5) of PBS solution.

The error bars in Figure 4 represent the method's reproducibility and robustness, which were measured independently and in the range of 21 ± 3 °C. RSD% values calculated from the standard deviation values in Figure 4 varied from 1.90% to 3.77% for 1, 10 and 100 fg/mL of S-AB. Those results imply the good reproducibility and robustness of the developed method. The stability and robustness of BSA/f-S-AG/CysNH<sub>2</sub>/Au/GCE were investigated by measuring the peak height at the end of

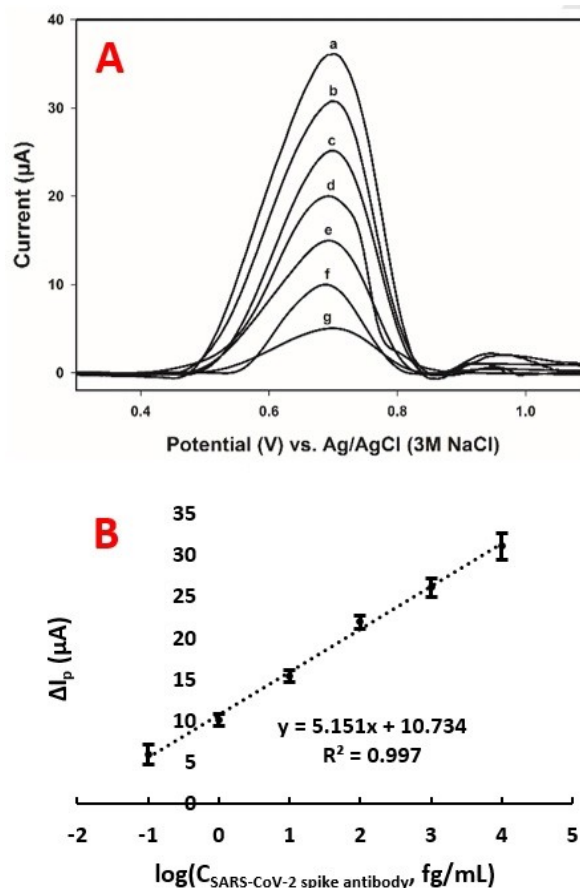


**Figure 4.** (A) The SWV voltammograms and (B) the calibration curve ( $n=3$  for each concentration) at BSA/f-S-AG/CysNH<sub>2</sub>/Au/GCE in 0.01 M (pH 7.5) of PBS solution. (a) 0.01 M (pH 7.5) of PBS solution, (b) + 0.1 fg/mL, (c) + 1 fg/mL, (d) + 10 fg/mL, (e) + 100 fg/mL, (f) + 1 pg/mL and (g) + 10 pg/mL of S-AB.

six 5-d periods at 4 °C, 25 °C and 37 °C, respectively (Figures S6 and S7). Although the difference between the results of storing the biosensor at 4 °C and 25 °C were not significant, the peak height of BSA/f-S-AG/CysNH<sub>2</sub>/Au/GCE maintained the signal from Day 1 (87.6%) even on Day 30 when stored at 37 °C. Those results indicate the excellent stability and robustness of BSA/f-S-AG/CysNH<sub>2</sub>/Au/GCE as well.

### Sample application

Non-spiked- and spiked-real samples originated from saliva and oropharyngeal swab were used to detect S-AB, and the recovery and relative standard deviation values obtained were 96.04%–97.47% and 2.34%–3.16%, respectively. The SWV voltammograms and results of the non-spiked- and spiked-real samples are shown in Figure S8, Figure S9 and Table 2. The results demonstrate that the method offers remarkable accuracy.

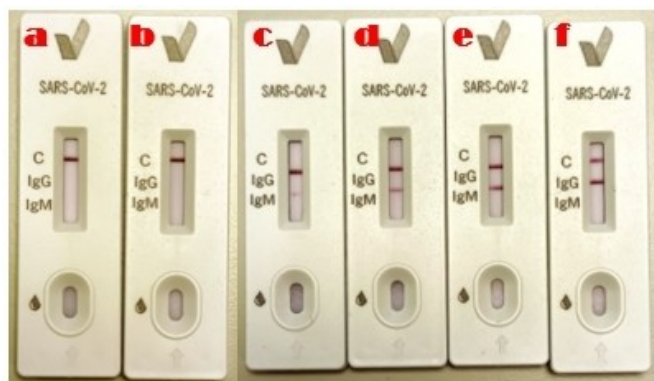
Different from our previous study,<sup>[3]</sup> LFIA method was compared with the proposed method in terms of sensitivity with different amount of S-AB appear in Figure 5. It was critical

Table 1. The interference studies for determining S-AB using BSA/f-S-AG/CysNH <sub>2</sub> /Au/GCE. Conditions: 100 fg/mL of S-AB, 0.01 M (pH 7.5) of PBS solution.		
Interference	Tolerable amount <sup>[a]</sup> (unit/mL)	Tolerable ratio <sup>[b]</sup>
α-amylase	300	–
Lipase	70	–
Na <sup>+</sup> , K <sup>+</sup>	–	600
Ca <sup>2+</sup> , Mg <sup>2+</sup>	–	500
H <sub>2</sub> PO <sub>4</sub> <sup>–</sup> , HCO <sub>3</sub> <sup>–</sup>	–	250
HPO <sub>4</sub> <sup>2–</sup> , urea	–	200
NH <sub>3</sub>	–	150

[a] Tolerable amount is the enzyme concentration directly in the assay medium. [b] Tolerable ratio is how many times more than 100 fg/mL (S-AB) of the interference does not change the peak height by more than 5%.

**Table 2.** The results of spiked-saliva and -oropharyngeal swab samples (n=6).

Sample	Added amount of S-AB (fg/mL)	S-AB found (mean $\pm$ standard deviation; fg/mL)	Recovery (%) (mean $\pm$ standard deviation)	Relative standard deviation (%)
Saliva	100	97.47 $\pm$ 2.29	97.47 $\pm$ 2.29	2.34
Oropharyngeal swab	100	96.04 $\pm$ 3.03	96.04 $\pm$ 3.03	3.16



**Figure 5.** Image obtained from LFIA cassettes at different concentration levels of S-AB. (a) 1 ng/mL, (b) 10 ng/mL, (c) 100 ng/mL, (d) 1  $\mu$ g/mL, (e) 10  $\mu$ g/mL and (f) 100  $\mu$ g/mL of S-AB.

to express that the LFIA method responded as a faint line at 100 ng/mL of S-AB and gave a negative response at lower concentrations (i.e. 1 and 10 ng/mL). The results clearly depicted that the developed biosensor was  $> 10^9$  times more sensitive than the LFIA method. Since patient individuals may have different virus levels and therefore different antibody levels, it was concluded that the proposed method can be utilized successfully for the early diagnosis of COVID-19.

A total of 40 samples marked positive (20 samples) or negative (20 samples) and confirmed by RT-PCR were randomly selected by TRaNS (Stratified Random Sample Selection) software to represent the stack and tested to evaluate the performance of the produced biosensor. To this end, 17/20 and 18/20 samples were in agreement with RT-PCR for negative and positive samples, respectively. The results depict the 85% specificity and 90% sensitivity of the produced biosensing platform.

## Conclusion

A rapid (approx.  $\sim$  20 min), accurate, inexpensive, easy-to-use, sensitive and selective immunosensing platform was developed and tested for detecting S-AB in spiked-saliva and -oropharyngeal swab samples via SWV. The developed biosensor proved to be the quickest to prepare among prominent electrochemical methods in the literature<sup>[3,41–50]</sup> and its results quicker to analyse.<sup>[3,42]</sup> In addition, the developed method surpassed RT-PCR in terms of inexpensiveness and time required for analysis,<sup>[12–19]</sup> which contribute to its relative simplicity. The developed biosensor, BSA/f-S-AG/CysNH<sub>2</sub>/Au/GCE, also offers a wide analytical range at the level of  $10^5$ . Compared to RT-PCR,

85% specificity and 90% sensitivity show that the accuracy of the method is quite satisfactory. Furthermore, using saliva and oropharyngeal swab samples without any preprocessing steps as in blood and serum samples may have facilitated the method's mentioned benefits. The fact that the developed biosensor did not show cross-reactivity, was not affected by interferences, was stable at different temperatures for a long time and yielded satisfactory results in real spiked-samples all suggest the good selectivity, robustness and accuracy of the proposed method. In addition, the proposed method has much better sensitivity than LFIA-based antibody tests. Moving forward, the developed biosensor could be easily fabricated as a ready-to-use kit on a commercial scale.

## Supporting Information Summary

Experimental section, electrochemical biosensing methods for determining SARS-CoV-2 and/or the related species, EDX spectra of the produced platforms, cyclic voltammetric characteristics of the system, optimisation studies, method validation and sample application results are demonstrated in the supporting information.

## Acknowledgements

This study was performed in the Electrochemistry Laboratory of TUBITAK UME. The authors would like to thank Sevgi Gülyüz at TUBITAK MAM-Materials Institute for SEM and EDX measurements and Tanıl Kocagöz for supplying the clinical samples which were formerly studied by RT-PCR.

## Conflict of Interest

The authors declare no conflict of interest.

## Data Availability Statement

The data that support the findings of this study are available in the supplementary material of this article.

**Keywords:** Antibody determination · biosensors · COVID-19 · gold · SARS-CoV-2

- [1] C. Sohrabi, Z. Alsafi, N. O'Neill, M. Khan, A. Kerwan, A. Al-Jabir, C. Iosifidis, R. Agha, *Int. J. Surg.* **2020**, *76*, 71–76.
- [2] F. Wu, S. Zhao, B. Yu, Y. M. Chen, W. Wang, Z. G. Song, Y. Hu, Z. W. Tao, J. H. Tian, Y. Y. Pei, M. L. Yuan, Y. L. Zhang, F. H. Dai, Y. Liu, Q. M. Wang, J. J. Zheng, L. Xu, E. C. Holmes, Y. Z. Zhang, *Nature* **2020**, *579*, 265–269.
- [3] L. Liv, *Microchem. J.* **2021**, *168*, 106445.

- [4] WHO, WHO coronavirus (COVID-19) dashboard. 2021, <https://covid19.who.int/>, 2021 (accessed 1 June 2021).
- [5] D. Wang, B. Hu, C. Hu, F. Zhu, X. Liu, J. Zhang, B. Wang, H. Xiang, Z. Cheng, Y. Xiong, Y. Zhao, Y. Li, X. Wang, Z. Peng, *JAMA* **2020**, *323*, 1061–1069.
- [6] N. Chen, M. Zhou, X. Dong, J. Qu, F. Gong, Y. Han, Y. Qiu, J. Wang, Y. Liu, Y. Wei, J. Xia, T. Yu, X. Zhang, L. Zhang, *Lancet* **2020**, *395*, 507–513.
- [7] M. Kenji, K. Katsushi, Z. Alexander, C. Gerardo, *Euro. Surveill.* **2020**, *25*, 2000180.
- [8] H. Nishiura, T. Kobayashi, T. Miyama, A. Suzuki, S. Jung, K. Hayashi, R. Kinoshita, Y. Yang, B. Yuan, A. R. Akhmetzhanov, N. M. Linton, *Int. J. Infect. Dis.* **2020**, *94*, 154–155.
- [9] D. P. Oran, E. J. Topol, *Ann. Intern. Med.* **2020**, *173*, 362–367.
- [10] P. Pokhrel, C. Hu, H. Mao, *ACS Sensors* **2020**, *5*, 2283–2296.
- [11] B. Udugama, P. Kadhiresan, H. N. Kozlowski, A. Malekjhani, M. Osborne, V. Y. C. Li, H. Chen, S. Mubareka, J. B. Gubbay, W. C. W. Chan, *ACS Nano* **2020**, *14*, 3822–3835.
- [12] P. Yang, D. Zhang, P. Yang, L. L. M. Poon, Q. Wang, *Lancet Infect. Dis.* **2020**, *20*, 411–412.
- [13] Y. Li, L. Yao, J. Li, L. Chen, Y. Song, Z. Cai, C. Yang, *J. Med. Virology* **2020**, *92*, 903–908.
- [14] J. F. Chan, C. C. Yip, K. K. To, T. H. Tang, S. C. Wong, K. H. Leung, A. Y. Fung, A. C. Ng, Z. Zou, H. Tsoi, G. K. Choi, A. R. Tam, V. C. Cheng, K. Chan, O. T. Tsang, K. Yuen, *J. Clin. Microbiol.* **2020**, *58*, e00310–20.
- [15] L. Lan, D. Xu, G. Ye, C. Xia, S. Wang, Y. Li, H. Xu, *JAMA* **2020**, *323*, 1502–1503.
- [16] S. W. Park, D. M. Cornforth, J. Dushoff, J. S. Weitz, *Epidemics* **2020**, *31*, 1–18.
- [17] P. B. Van Kasteren, B. van der Veer, S. van den Brink, L. Wijsman, J. de Jonge, A. van den Brandt, R. Molenkamp, C. B. E. M. Reusken, A. Meijer, *J. Clin. Virol.* **2020**, *128*, 104412.
- [18] M. Yang, S. Chen, B. Huang, J. M. Zhong, H. Su, Y. J. Chen, Q. Cao, L. Ma, J. He, X. Li, X. Li, J. Zhou, J. Fan, D. Luo, X. Chang, K. Arkun, M. Zhou, X. Nie, *Eur. Urol. Focus* **2020**, *6*, 1124–1129.
- [19] B. Visseaux, Q. Le Hingrat, G. Collin, D. Bouzid, S. Lebourgeois, D. Le Pluart, L. Deconinck, F. Lescure, J. Lucet, L. Bouadma, J. Timsit, D. Descamps, Y. Yazdanpanah, E. Casalino, N. Houhou-Fidouh, *J. Clin. Microbiol.* **2020**, *58*, e00630–20.
- [20] J. P. Broughton, X. Deng, G. Yu, C. L. Fasching, V. Servellita, J. Singh, X. Miao, J. A. Streithorst, A. Granados, A. Sotomayor-Gonzalez, K. Zorn, A. Gopez, E. Hsu, W. Gu, S. Miller, C. Pan, H. Guevara, D. A. Wadford, J. S. Chen, C. Y. Chiu, *Nat. Biotechnol.* **2020**, *38*, 870–874.
- [21] D. Wang, S. He, X. Wang, Y. Yan, J. Liu, S. Wu, S. Liu, Y. Lei, M. Chen, L. Li, J. Zhang, L. Zhang, X. Hu, X. Zheng, J. Bai, Y. Zhang, Y. Zhang, M. Song, Y. Tang, *Nat. Biomed. Eng.* **2020**, *4*, 1150–1158.
- [22] B. G. Andryukov, *AIMS Microbiol.* **2020**, *6*, 280–304.
- [23] C. Huang, T. Wen, F. J. Shi, X. Y. Zeng, Y. J. Jiao, *ACS Omega* **2020**, *5*, 12550–12556.
- [24] L. Zeng, Y. Li, J. Liu, L. Guo, Z. Wang, X. Xu, S. Song, C. Hao, L. Liu, M. Xin, C. Xu, *Mater. Chem. Front.* **2020**, *4*, 2000–2005.
- [25] Z. Chen, Z. Zhang, X. Zhai, Y. Li, L. Lin, H. Zhao, L. Bian, P. Li, L. Yu, Y. Wu, G. Lin, *Anal. Chem.* **2020**, *92*, 7226–7231.
- [26] X. Li, Q. Zhang, P. Hou, M. Chen, W. Hui, A. Vermorken, Z. Luo, H. Li, Q. Li, Y. Cui, *Int. J. Mol. Med.* **2015**, *36*, 1319–1326.
- [27] T. Wen, C. Huang, F. J. Shi, X. Y. Zeng, T. Lu, S. N. Ding, Y. J. Jiao, *Analyst* **2020**, *145*, 5345–5352.
- [28] F. W. Chow, T. T. Chan, A. R. Tam, S. Zhao, W. Yao, J. Fung, F. K. Cheng, G. C. Lo, S. Chu, K. L. Aw-Yong, J. Y. Tang, C. Tsang, H. K. Luk, A. C. Wong, K. S. Li, L. Zhu, Z. He, E. W. T. Tam, T. W. Chung, S. C. Y. Wong, T. Que, K. S. Fung, D. C. Lung, A. K. Wu, I. F. Hung, P. C. Woo, S. K. Lau, *Int. J. Mol. Sci.* **2020**, *21*, 5380.
- [29] M. Jiang, W. Pan, A. Arasther, W. Fang, L. Ling, H. Fang, F. Daneshnia, J. Yu, W. Liao, H. Pei, X. Li, C. Lass-Floerl, *Front. Cell. Infect. Mi.* **2020**, *10*, 331.
- [30] C. Yan, J. Cui, L. Huang, B. Du, L. Chen, G. Xue, S. Li, W. Zhang, L. Zhao, Y. Sun, H. Yao, N. Li, H. Zhao, Y. Feng, S. Liu, Q. Zhang, D. Liu, J. Yuan, *Clin. Microbiol. Infect.* **2020**, *26*, 773–779.
- [31] T. Yang, Y. C. Wang, C. F. Shen, C. M. Cheng, *Diagnostics* **2020**, *10*, 165.
- [32] X. Ding, K. Yin, Z. Li, R. V. Lalla, E. Ballesteros, M. M. Sfeir, C. Liu, *Nat. Commun.* **2020**, *11*, 4711.
- [33] X. Wang, M. Zhong, Y. Liu, P. Ma, L. Dang, Q. Meng, W. Wan, X. Ma, J. Liu, G. Yang, *Sci. Bull.* **2020**, *65*, 1436–1439.
- [34] Z. Huang, D. Tian, Y. Liu, Z. Lin, C. J. Lyon, W. Lai, D. Fusco, A. Drouin, X. Yin, T. Hu, B. Ning, *Biosens. Bioelectron.* **2020**, *164*, 112316.
- [35] E. R. Adams, R. Anand, M. I. Andersson, K. Auckland, J. K. Baillie, E. Barnes, S. Beer, J. I. Bell, T. Berry, S. Bibi, M. Carroll, S. Chinnakannan, E. Clutterbuck, R. J. Cornell, D. W. Crook, T. De Silva, W. Dejnirattisai, K. E. Dingle, C. Dold, A. Espinosa, D. W. Eyre, H. Farmer, M. F. Mendoza, D. Georgiou, S. J. Hoosdally, A. Hunter, K. Jeffrey, P. Klenerman, J. Knight, C. Knowles, A. J. Kwok, U. Leuschner, R. Levin, C. Liu, C. Lopez-Camacho, J. C. M. Garrido, P. C. Matthews, H. McGivern, A. J. Mentzer, J. Milton, J. Mongkolsapaya, S. C. Moore, M. S. Oliveira, F. Pereira, E. P. Lopez, T. Peto, R. J. Ploeg, A. Pollard, T. Prince, D. J. Roberts, J. K. Rudkin, V. Sanchez, G. R. Screaton, M. G. Semple, D. T. Skelly, J. Slon-Campos, E. N. Smith, A. J. S. Diaz, J. Staves, D. Stuart, P. Supasa, T. Surik, H. Thraves, P. Tsang, L. Turtle, A. S. Walker, B. Wang, C. Washington, N. Watkins, J. Whitehouse, *medRxiv* **2020**, 04.15.20066407.
- [36] E. Karakuş, E. Erdemir, N. Demirbilek, L. Liv, *Anal. Chim. Acta* **2021**, *1182*, 338939.
- [37] Y. Fang, H. Zhang, J. Xie, M. Lin, L. Ying, P. Pang, W. Ji, *Radiology* **2020**, *296*, E115–E117.
- [38] G. Qiu, Z. Gai, Y. Tao, J. Schmitt, G. A. Kullak-Ublick, J. Wang, *ACS Nano* **2020**, *14*, 5268–5277.
- [39] A. Ahmadvand, B. Gerisliloglu, Z. Ramezani, A. Kaushik, P. Manickam, S. A. Ghoreishi, *arXiv* **2020**, 2006.08536.
- [40] B. E. Fan, V. C. L. Chong, S. S. W. Chan, G. H. Lim, K. G. E. Lim, G. B. Tan, S. S. Muehli, P. Kuperan, K. H. Ong, *Am. J. Hematol.* **2020**, *95*, E131–E134.
- [41] M. Alafeef, K. Dighe, P. Moitra, D. Pan, *ACS Nano* **2020**, *14*, 17028–17045.
- [42] L. Fabiani, M. Saroglia, G. Galatà, R. De Santis, S. Fillo, V. Luca, G. Faggioni, N. D'Amore, E. Regalbuto, P. Salvatori, G. Terova, D. Moscone, F. Lista, F. Arduini, *Biosens. Bioelectron.* **2020**, *171*, 112686.
- [43] G. Seo, G. Lee, M. J. Kim, S. Baek, M. Choi, K. B. Ku, C. Lee, S. Jun, D. Park, H. G. Kim, S. Kim, J. Lee, B. T. Kim, E. C. Park, S. I. Kim, *ACS Nano* **2020**, *14*, 5135–5142.
- [44] R. M. Torrente-Rodríguez, H. Lukas, J. Tu, J. Min, Y. Yang, C. Xu, H. B. Rossiter, W. Gao, *Matter* **2020**, *3*, 1–18.
- [45] B. S. Vadlamani, T. Uppal, S. C. Verma, M. Misra, *Sensors* **2020**, *20*, 5871.
- [46] H. Zhao, F. Liu, W. Xie, T. C. Zhou, J. OuYang, L. Jin, H. Li, C. Y. Zhao, L. Zhang, J. Wei, Y. Zhang, C. Li, *Sens. Actuators B Chem.* **2021**, *327*, 128899.
- [47] Z. Rahmati, M. Roushani, H. Hosseini, H. Choobin, *Microchim. Acta* **2021**, *188*, 105.
- [48] B. Mojsoska, S. Larsen, D. A. Olsen, J. S. Madsen, I. Brandslund, F. A. Alatraktchi, *Sensors* **2021**, *21*, 390.
- [49] S. Eissa, M. Zourob, *Anal. Chem.* **2021**, *93*, 1826–1833.
- [50] L. Liv, G. Çoban, N. Nakiboğlu, T. Kocagöz, *Biosens. Bioelectron.* **2021**, *192*, 113497.
- [51] L. Liv, M. Yener, G. Çoban, Ş. A. Can, *Anal. Bioanal. Chem.* **2022**, *414*, 1313–1322.
- [52] L. M. Kucirka, S. A. Lauer, O. Laeyendecker, D. Boon, J. Lessler, *Ann. Intern. Med.* **2020**, *173*, 262–267.
- [53] T. Ai, Z. Yang, H. Hou, C. Zhan, C. Chen, W. Lv, Q. Tao, Z. Sun, L. Xia, *Radiology* **2020**, *296*, E32–E40.
- [54] X. L. Wang, H. P. Yao, X. Xu, P. Y. Zhang, M. M. Zhang, J. B. Shao, Y. Q. Xiao, H. L. Wang, *Clin. Chem.* **2020**, *66*, 977–979.
- [55] Z. Ye, Y. Zhang, Y. Wang, Z. Huang, B. Song, *Eur. Radiol.* **2020**, *30*, 4381–4389.
- [56] M. S. Khan, S. K. Misra, K. Dighe, Z. Wang, A. S. Schwartz-Duval, D. Sar, D. Pan, *Biosens. Bioelectron.* **2018**, *110*, 132–140.
- [57] M. S. Khan, K. Dighe, Z. Wang, I. Srivastava, A. S. Schwartz-Duval, S. K. Misra, D. Pan, *Analyst* **2019**, *144*, 1448–1457.
- [58] F. Liu, K. S. Choi, T. J. Park, S. Y. Lee, T. S. Seo, *BioChip J.* **2011**, *5*, 123–128.
- [59] R. Wang, C. Xue, M. Gao, H. Qi, C. Zhang, *Microchim. Acta* **2011**, *172*, 291–297.
- [60] L. A. Layqah, S. Eissa, *Microchim. Acta* **2019**, *186*, 224.
- [61] J. Abbasi, *JAMA* **2021**, *326*, 1781–1782.
- [62] G. Liu, J. F. Rusling, *ACS Sensors* **2021**, *6*, 593–612.

Submitted: January 20, 2022

Accepted: March 1, 2022